

Effects of wintertime haze on regional thermal environment and urban heat island in the Yangtze River Delta, China



Quan Zhang^a, Lang Liu^b, Gang Yang^{a,c}, Weiwei Sun^{a,c,*}, Huimin Lu^d, Tian Feng^{a,c,*}

^a Department of Geography & Spatial Information Techniques, Ningbo University, Ningbo, China

^b School of Public Policy and Administration, Northwestern Polytechnical University, Xi'an, China

^c Institute of East China Sea, Ningbo University, Ningbo, China

^d School of Civil Engineering and Architecture, College of Science & Technology Ningbo University, China

ARTICLE INFO

Keywords:

UHI
Haze pollution
PM_{2.5} components
WRF-Chem

ABSTRACT

Urban heat island (UHI) is an important issue of regional thermal environment in urban climate, which is affected by airborne particulates. However, the influences of various aerosol compositions on the UHI have been rarely reported. This study investigates the radiative effects of particulates on regional thermal environment and the UHI intensity (UHII) in the YRD during January 2018 using the WRF-Chem model. The model performs reasonably in reproducing the observed evolutions of the key meteorological fields and air pollutants. Our results show that the UHI effect is prevalent over megacities of the YRD, with markedly higher surface UHII compared to the canopy one. The UHI effect generally gets more significant during nighttime and reaches the maximum in the late afternoon. Fine particulates nonlinearly reduce the surface and air temperature, which lowers the UHII throughout the day, but significant differences exist among different UHI indices. We highlight that these influences are predominantly attributed to the radiative effect of sulfate, nitrate, and ammonium aerosols. As a comparison, the effects of organic aerosols are much less and black carbon reduces the UHI almost negligibly. This study would contribute to a comprehensive understanding of radiative effects of aerosols on the UHI.

1. Introduction

Fine particulate matter, i.e., particles with an aerodynamic diameter no more than 2.5 μm (PM_{2.5}), is one of the most critical pollutants in deteriorating air quality (Feng et al., 2020; Gu et al., 2018; Tiwari et al., 2014; Xing et al., 2017). The accumulation of a large number of fine particles is the direct cause of haze weather, which exerts negative impacts on human health and the ecosystem (Diao et al., 2021; Lin et al., 2016; Sulong et al., 2017). Specifically, it has been pointed that air pollution with high levels of airborne particles may significantly affect the regional thermal environment, the boundary layer structure, and hence the urban heat island (UHI) effect through aerosol radiative effect (Han et al., 2020; Li et al., 2020; Miao et al., 2019; Sun et al., 2013; Yang et al., 2020a). The Yangtze River Delta (YRD) region is one of the regions characterized by high particulate concentrations in China (Hu and Brunsell, 2015; Ming et al., 2017), but the effects of haze pollution on regional thermal environment and the UHI still remain to be elucidated.

Regional thermal environment, generally represented by surface temperature and air temperature, is an important parameter in

* Corresponding authors at: Department of Geography & Spatial Information Techniques, Ningbo University, Ningbo, China.
E-mail addresses: sunweiwei@nbu.edu.cn (W. Sun), fengtian@nbu.edu.cn (T. Feng).

radiation balance and surface physical process in the surface-atmosphere coupling system (Li et al., 2013a; Li et al., 2013b), which plays a key role in the UHI effect (Estoque et al., 2017; Peng et al., 2016; Sheng et al., 2017; Zhou et al., 2013). UHI refers to a regional climate effect that is characterized by high temperature in urban areas and lower in suburban and non-urban areas (Oke, 1982). In terms of the vertical height of the temperature, there are generally different types of UHI. The surface UHI (SUHI), characterized by surface temperature, is the most widely used proxy for the UHI (Clinton and Gong, 2013; Peng et al., 2012; Zhou et al., 2018). Besides that, the atmospheric UHI and canopy UHI (CUHI) are selected to represent the UHI at higher elevations (Deilami et al., 2018; Gago et al., 2013; Hu and Brunsell, 2015; Pichierri et al., 2012; Wang et al., 2017). Several pathways have been implemented to explore the UHI. In early studies, researchers use observational data from meteorological stations to uncover the UHI owing to the accessibility. This method performs well in understanding the intensity, the long-term evolution, and the diurnal variation of the UHI (Fenner et al., 2014; Wang et al., 2020; Yang et al., 2020b). Satellite remote sensing is another important measure to access the UHI, particularly in investigating regional and even global UHI, which has gradually become a predominant tool in the study of UHI (Clinton and Gong, 2013; Li et al., 2013b; Zhou et al., 2018; Zhou et al., 2014). In addition, the involvement of atmospheric transport models also can be used to understand both the phenomenon and the underlying physical mechanism of the UHI (Bhati and Mohan, 2015; Chew et al., 2021; Cui and de Foy, 2012; Li et al., 2020; Singh et al., 2022). Recent studies indicated that wind speed is negatively correlated with the CUHI (Chen et al., 2022). The effects of natural variability and anthropogenic heat flux on air temperature are more complex. Different synoptic situations cause changes in the UHI through modulation of local meteorological factors and human activities bring changes in daily temperature, and hence the UHI (Yang et al., 2020a; Yang et al., 2022).

Regional thermal environment can be also modulated by air pollutions significantly, which as a result lead to changes in the UHI (Wang et al., 2021). Air pollutions with high levels of airborne particulates have a strong aerosol radiative forcing effect via absorbing and scattering incident solar radiations (Bi et al., 2014; Zhang et al., 2020). For example, Chen et al. (2018) found that the UHI intensity (UHII) increased by 16.7% during the more severe haze episodes in winter compared to in other seasons in Beijing. Yang et al. (2020b) reported that the haze pollution weakened the UHI effect in Beijing at night in both summer and winter, but strengthened it during daytime in winter based on ground sounding data from 2016 to 2018. In addition, Hereher et al. (2022) analyzed the relationship between SUHII and the concentrations of different air pollutants (NO_2 , SO_2 , CO) in Cairo region and found the highest correlation between NO_2 and SUHII in spring ($R^2 = 0.59$), but there were significant differences among seasons. However, to date, the influence of haze pollution on the UHI is still controversial among different studies. A positive correlation between haze pollution and the UHII is reported in Thessaloniki, Greece during summertime (Poupkou et al., 2011). Likewise, in the Beijing-Tianjin-Hebei region, Yang et al. (2020a) also presented that the UHII increases with the $\text{PM}_{2.5}$ concentration based on daily observations in winter. On the contrary, some researches also show that the accumulation of fine particles may lead to an imbalance of energy in the boundary layer over the city, resulting in an “urban cold island” (Christoforou et al., 2000; Sang et al., 2000). Further, ambient $\text{PM}_{2.5}$ is mainly composed of sulfate, nitrate, and ammonium aerosols (SNA), organic aerosols (ORG), and black carbon (BC). These species originate from primary emissions of natural and anthropogenic sources and secondary physicochemical formations of precursors. Different aerosol components differ significantly in radiative effects (Seinfeld and Pandis, 2006), exerting distinct impacts on surface thermal environment and the UHI. Generally, SNA (BC) has a strong scattering (absorbing) property, and the radiative effect of ORG is between SNA and BC (Athanasopoulou et al., 2013; Liousse et al., 1996; Slater et al., 2022; Xu and Penner, 2012).

The urban agglomeration in the YRD region is large and densely populated, and the urban-scale climate effect is obvious (Cheng et al., 2020; Wang et al., 2022; Zhan and Xie, 2022; Zhang et al., 2021a; Zhang et al., 2021b). The phenomenon of UHI in the YRD has existed for a long time (Du et al., 2007; Shen et al., 2020), and $\text{PM}_{2.5}$ pollution in the YRD gets worst during wintertime in a year (Ming et al., 2017; Zhang et al., 2019). Studies have also reported the impacts of airborne particulates on the UHI in this region. For example, Song et al. (2018) reported that the surface temperature in Shanghai was affected by ambient $\text{PM}_{2.5}$ more than by vegetation coverage from 2001 to 2006. Zhong et al. (2017a) found that aerosol had a regional cooling effect in both summer and winter in the YRD region using the WRF-Chem model coupled with a single layer urban canopy model. Some other studies also showed that ambient haze pollution reduced regional shortwave radiation, which led to a decrease in surface temperature (Che, 2005; Qian et al., 2006; Qian et al., 2007). However, studies on the influences of various aerosol compositions upon regional thermal environment and the UHI in this region have been rarely reported.

Therefore, in this study, we examine the influence of different types of ambient particulate matter on regional thermal environment and the UHI effect in winter in the YRD region using the WRF-Chem model. Section 2 describes the configuration of the model and adopted data, Section 3 presents the main results and discussion, and the conclusions are summarized in Section 4.

2. Model and methods

The flow framework of the present study is depicted in Fig. S1. The baseline simulation of the WRF-Chem model is validated using observational data from air monitoring sites, weather stations, and the MODIS satellite retrievals. Four sensitivity experiments are performed based on the baseline simulation to investigate the effects of $\text{PM}_{2.5}$, SNA, ORG, and BC on thermal temperature environment and the UHI.

2.1. Model and configurations

In this study, we used a specific version of the WRF-Chem model developed by Li et al. (Li et al., 2011a; Li et al., 2012; Li et al., 2011b), which is based on the official release developed by the National Center for Atmospheric Sciences (NCAR) and the National Oceanic and Atmospheric Administration (NOAA) (Grell et al., 2005). This version develops a flexible gas phase chemistry module (Li

et al., 2011a; Li et al., 2012; Li et al., 2011b). Considering the photochemical effects of clouds and aerosols, the fast tropospheric ultraviolet and visible radiation (FTUV) module was incorporated in the calculation of the photolysis rate (Li et al., 2005; Tie et al., 2003). The Models-3 Community Multiscale Air Quality (CMAQ) aerosol model developed by the US Environmental Protection Agency is added to the model to simulate aerosol chemistry and physics (Binkowski and Roselle, 2003). The ISORROPIA (version 1.7) (Nenes et al., 1998) and a SO₂ heterogeneous reaction parameterization reported by Li et al. (2017) are also included in calculation of inorganic aerosols. The simulation of organic aerosols uses the volatility basis-set (VBS) approach (Donahue et al., 2006; Robinson Allen et al., 2007), in which the formation of secondary organic aerosol (SOA) includes the contribution from glyoxal and methyl-glyoxal (Volkamer et al., 2007; Zhao et al., 2006). The short and long-wave radiation is simulated with the New Goddard radiation scheme, which considers the aerosol radiative effects (Chou and Suarez, 1999). The dry deposition of chemical substances was parameterized according to Wesely (2007), and the wet deposition was calculated following the treatment in the CMAQ module (Binkowski and Roselle, 2003).

The simulation area is the YRD region (Fig. 1), which consists of 200 × 200 grid cells with a spatial resolution of 6 km × 6 km. The center is located at 31.2°N, 120.0°E. The simulation period is January 2018, and the first three days are used as the spin-up time. The NCEP (National Centers for Environmental Prediction) FNL reanalysis data with a resolution of 1° × 1° are used as initial and boundary conditions of the meteorological fields. The initial and boundary conditions of the chemical fields come from the output of Model for Ozone And Related chemical Tracers (MOZART) with a 6 h interval (Horowitz et al., 2003). The anthropogenic emission inventory uses the MEIC inventory with a resolution of 0.25° × 0.25° (http://meicmodel.org/?page_id=560). Biogenic emissions are calculated using the Model of Emissions of Gases and Aerosol from Nature (MEGAN) online. Table 1 shows more details about the model configuration.

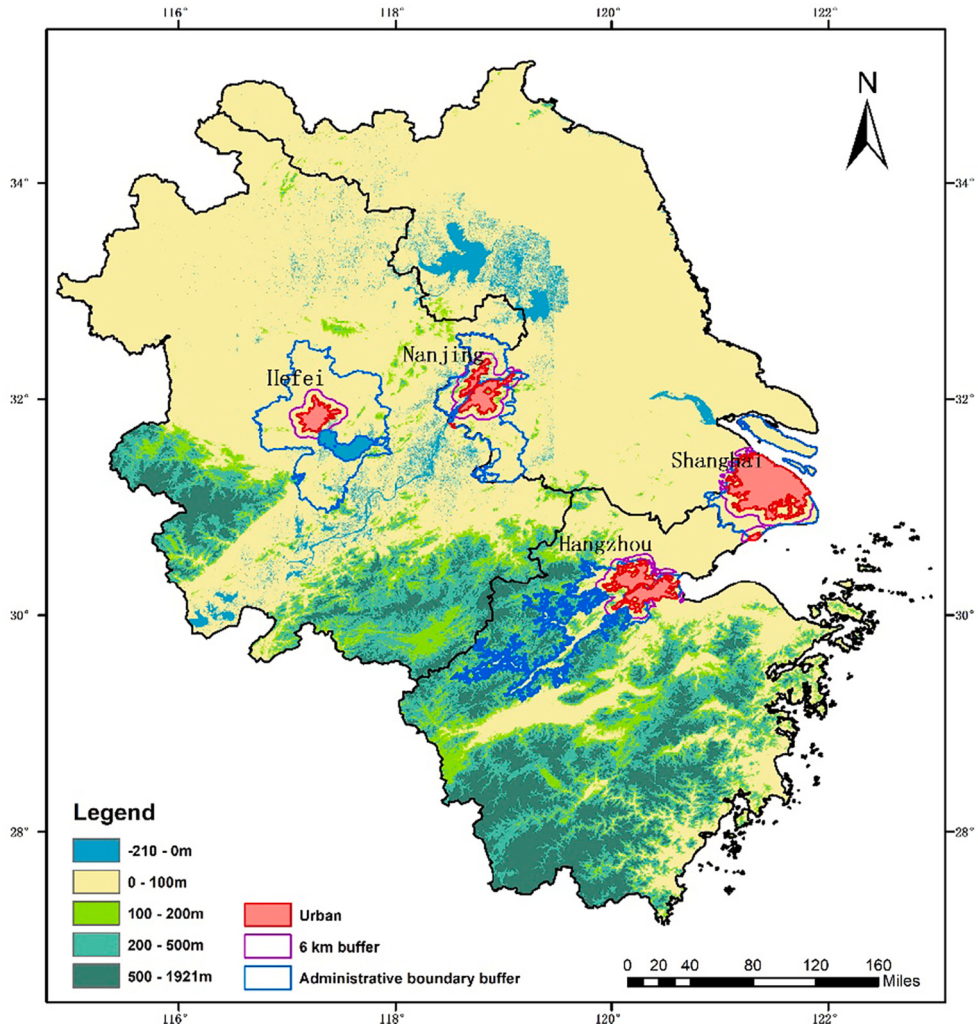


Fig. 1. Map showing the study domain with topography, in which urban and different buffer areas are explicitly marked. The pink areas show urban areas of the largest four megacities over this region, i.e., Shanghai, Nanjing, Hangzhou, and Hefei. Red and blue curves denote the urban buffer areas represented by a 6 km distance away from the urban areas and by the administrative boundaries, respectively. (For interpretation of the references to colour in this figure legend, the reader is referred to the web version of this article.)

2.2. Calculation of UHI

In this study, we select two kinds of urban buffer areas to calculate the UHI. Studies have proposed that a fraction of 50% to 300% of the built-up area can be used as the urban buffer zone (Yao et al., 2018). Following this treatment, the areas within 6 km away from the built-up area are selected as the urban buffer, which is intuitive and has been widely used in previous studies (Clinton and Gong, 2013). In the other approach, considering that administrative divisions themselves have a stronger practical significance, the urban buffer is extended to the administrative boundary, which reflects the impact of human activities on regional thermal environment. In both approaches, water bodies, wetlands, and areas with a height difference greater than 50 m from the built-up area are not included (Lai et al., 2018; Yao et al., 2018). We adopt these two methods in the calculation of the UHII through differentiating the temperature between the built-up areas and the urban buffer zone. Therefore, the UHII is estimated using the following equations:

$$\text{UHII}_{6\text{km}} = T_u - T_{6\text{km}} \quad (1)$$

$$\text{UHII}_{\text{bdr}} = T_u - T_{\text{bdr}} \quad (2)$$

where $\text{UHII}_{6\text{km}}$ and UHII_{bdr} indicate that the UHII is calculated using a 6 km buffer zone and the administrative boundary, respectively. T_u is temperature in the built-up areas, and $T_{6\text{km}}$ and T_{bdr} denote the temperature in the urban buffer zone implemented by a 6 km distance and the administrative boundary, respectively. If surface temperature is adopted in the calculation, the obtained UHII is surface UHII (SUHII), and else if air temperature at 2 m is adopted, the obtained UHII is canopy UHII (CUHII).

2.3. Satellite data and air pollutant measurements

The land use data come from the MODIS satellite MCD12Q1 product (<https://modis-land.gsfc.nasa.gov/landcover.html>), which was mainly used to extract urban areas in the YRD region in 2018. Urban patches with an area less than 50 km² are not considered, and water bodies and wetlands are also not included. The elevation data from ASTER (The Advanced Spaceborne Thermal Emission and Reflection Radiometer) GDEMv2 (Global Digital Elevation Model), with a resolution of 30 m, are mainly used to eliminate the urban buffer zone with an elevation difference of more than 50 m (<https://www.gscloud.cn/sources/accessdata/421?pid=302>). The MOD11A2 v6 Terra land surface temperature products from Google Earth Engine during the period of January 9–16, 2018 for surface temperature comparisons with the model. The MOD11A2 v6 product provides an 8-day average land surface temperature and emissivity with a spatial resolution of 1 km by 1 km.

Observations at eight weather stations in the YRD are used to evaluate the model performance in predicting meteorological fields, which includes the Hongqiao station in Shanghai (31.19°N, 121.33°E), the Xiaoshan station in Hangzhou (30.14°N, 120.10°E), the Lukou station in Nanjing (31.56°N, 118.54°E), the Luogang station in Hefei (31.47°N, 117.18°E), the Anqing station (30.61°N, 116.96°E), the Chun'an station (29.61°N, 119.01°E), the Dongtai station (32.85°N, 120.28°E), and the Huaiyin station (33.63°N, 118.93°E). These weather stations provided routine meteorological parameters including air temperature and relative humidity at 2 m and wind speed and direction at 10 m. The time interval is 1 h for the Hongqiao, Xiaoshan, Lukou, and Luogang stations, 3 h for the Anqing, Dongtai and Huaiyin stations, and 6 h for the Chun'an station. To validate the model performance in simulating chemical species, we use hourly PM_{2.5} measurements from 227 ambient air monitoring stations in the YRD region (9 in Shanghai, 55 in Zhejiang, 97 in Jiangsu, and 66 in Anhui) during January 2018. These data are obtained from the Ministry of Ecology and Environment of China (available at <https://air.cnemc.cn:18007> or <http://www.aqistudy.cn>). In addition, the measurements from the Dianshan Lake station

Table 1
Model configurations.

Item	Configuration
Period	January 2018
Region	The Yangtze River Delta, China
Domain center	31.2°N, 120.0°E
Domain size	900 km × 900 km
Horizontal resolution	6 km × 6 km
Vertical resolution	35 vertical levels with a stretched vertical grid with spacing ranging from 50 m near surface, to 500 m at 2.5 km and 1 km above 14 km
Microphysics scheme	WRF Single-Moment 6-class scheme (Song-You and Jeong-Ock Jade, 2006)
Boundary layer scheme	MYJ TKE scheme (Janić, 2002)
Surface layer scheme	MYJ surface scheme (Janić, 2002)
Land-surface scheme	Noah land surface model (Chen and Dudhia, 2001)
Longwave radiation scheme	New Goddard scheme (Chou et al., 2001)
Shortwave radiation scheme	New Goddard scheme (Chou and Suarez, 1999)
Meteorological boundary and initial condition	NCEP 1° × 1° reanalysis data
Chemical boundary and initial condition	MOZART 6 h output (Horowitz et al., 2003)
Anthropogenic emission inventory	SAPRC99 chemical mechanism emissions (Li et al., 2017; Zhang et al., 2009b)
Biogenic emission inventory	MEGAN model developed by Guenther et al. (2006)
Spin-up time	3 days

in Jiangsu (120.99°N, 31.18°E) is used to evaluate the simulations of the main aerosol compositions in ambient PM_{2.5}. More details about the measurements have been previously reported by Sun et al. (2019). The ions including sulfate, nitrate, and ammonium are measured using a MARGA instrument (ADI 2080, Applikon Analytical, Netherlands) and the detection limits are 0.04 µg m⁻³, 0.05 µg m⁻³, and 0.09 µg m⁻³, respectively. The OC and EC concentrations are obtained with a Sunset semi-continuous carbon analyzer (Sunset Laboratory, Forest Grove, Oregon, USA) using thermal and optical methods. More detailed information about the instruments is found in Sun et al. (2019). For the comparison convenience, a factor of 1.8 is used to translate OC to organic aerosol (OA) (Finessi et al., 2012; McDonald et al., 2015).

3. Results and discussion

3.1. Model evaluation

3.1.1. Meteorological fields

The meteorological fields play a key role in the evolution of the spatial and temporal patterns of gas-phase and particulate pollutants (He et al., 2017; Zhang et al., 2022). To assess the model simulation performance against observations, three statistical parameters are introduced, including mean bias (MB), root mean square error (RMSE), and index of agreement (IOA), which are defined as follows:

$$\text{MB} = \frac{\sum_{i=1}^N (P_i - O_i)}{\sum_{i=1}^N O_i} \quad (3)$$

$$\text{RMSE} = \left[\frac{1}{N} \sum_{i=1}^N (P_i - O_i)^2 \right]^{\frac{1}{2}} \quad (4)$$

$$\text{IOA} = 1 - \frac{\sum_{i=1}^N (P_i - O_i)^2}{\sum_{i=1}^N (|P_i - \bar{O}| + |O_i - \bar{O}|)^2} \quad (5)$$

In these equations, P_i and O_i represent simulation and observation variables, N is the total time used for comparison, \bar{O} represents the average of observation variables. IOA ranges from 0 to 1, and a higher value means better simulation performance.

Figs. S2 and S3 show a comparison between the modeled and observed temporal variations of air temperature and relative humidity. Observations at the weather stations show that the daily maximum air temperature is uniformly about 12.0 °C – 16.1 °C in this region, but the daily minimum air temperature varies remarkably among these stations, ranging from –11.0 °C to –1.5 °C. The model performs reasonably well in replicating the temporal profiles of air temperature with IOAs ranging from 0.92 to 0.95 at the Hongqiao, Xiaoshan, Lukou, Dongtai, and Huaiyin stations. Moderate underestimation occurs at the Luogang and Anqing stations (MB of –2.2 and –2.1, respectively), and overestimation occurs at the Chun'an station (MB = 2.0), but the model can still reproduce the fluctuation of air temperature with an IOA of 0.81–0.86. The observed relative humidity varies significantly during the first half period, and stays high in the second half. The model simulation captures the frequent fluctuations at the Hongqiao, Xiaoshan, Dongtai, Huaiyin stations reasonably (IOA of 0.84 and 0.89, respectively), but overestimates exist during the first half period at the Lukou, Luogang and Anqing stations.

Figs. S4 and S5 present a comparison between the simulated and observed wind fields at the eight weather stations. The observations show that northerly wind prevailed during the simulation period in the YRD region, and the highest wind speed reached about 10 m s⁻¹. The modeled temporal profiles of wind directions are in good agreement with the observations (IOA of 0.72–0.98). Although the model shows some deviations in Chun'an and Dongtai (IOA of 0.52 and 0.67, respectively), it still yields the temporal variations well for the other sites (IOA of 0.71–0.84).

We further evaluate the modeled surface temperature against satellite retrievals. Fig. S6 shows the comparison of the model simulated surface temperature and the surface temperature from the MODIS satellite remote sensing product (MOD11A2). Considering the observational time (around 10:30 LT) of the satellite in the study area, we compare the model result averaged over 10:00 and 11:00 LT with the satellite data. Due to the cloud cover issue in satellite retrievals, only the data spanning January 9–16, 2018 are selected. The satellite data generally show an increasing gradient from northwest to southeast in wintertime surface temperature over the YRD, which is reasonably captured by the model. Relatively large biases in simulated surface temperature occur in the northwest part of the area.

3.1.2. Haze pollutions

To assess the model simulation in the haze pollutions, we compare the simulated surface PM_{2.5} concentrations with observations in the YRD area. Fig. 2 shows the temporal variations of the simulated PM_{2.5} concentrations against observations which are averaged over the monitoring stations in each province (municipality) of the YRD region. The observations show that the YRD region experienced several severe haze events during January 2018 and the maximum PM_{2.5} concentration reached 200 µg m⁻³ and even higher. In

particular, a heavy and persistent haze pollution occurred during the period from January 17 to 23, which is well captured by the WRF-Chem model. Statistics shows that, for the whole period, the model can reasonably reproduce the temporal profiles of the observed PM_{2.5} concentrations (IOAs of 0.84–0.92), although discrepancies still exist occasionally, especially around January 10 and January 23. Figs. S7 and S8 demonstrate PM_{2.5} concentrations on January 10–12 and 22–23, respectively, where the wind field plays an important role in the accumulation and dispersion of air pollutants (He et al., 2017), and pollution transmission from upstream areas (Henan and Shandong) contributes to the PM_{2.5} overestimation (especially in Anhui). Fig. 3 illustrates the spatial distributions of the simulated and observed PM_{2.5} concentrations averaged over the study period in the YRD region. The observation shows higher PM_{2.5} concentrations in the northwestern cities and lower concentrations in the southeastern cities of the YRD region. This spatial pattern is well replicated by the model simulation, which presents a clear southeast-to-northwest gradient in PM_{2.5} concentration. Overall, the stagnant air corresponds to higher PM_{2.5} concentrations in the northwestern part of YRD and prevailing northerly winds from the ocean tie in with lower PM_{2.5} levels in the eastern and southern parts.

Fig. 4 further presents a comparison between the simulated and measured chemical compositions of ambient PM_{2.5} at the Dianshan

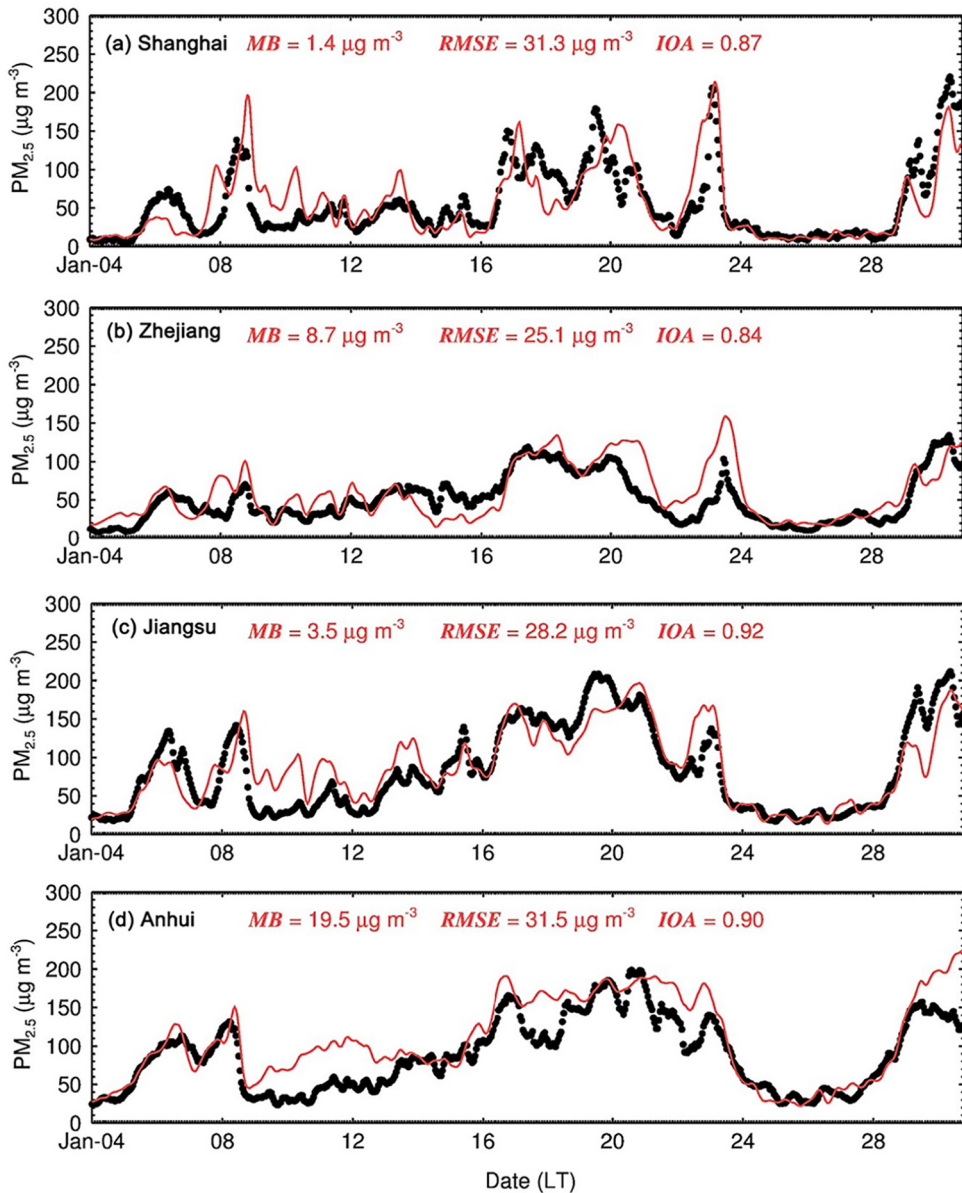


Fig. 2. Temporal variations of simulated (red curves) and measured (black dots) near-surface PM_{2.5} concentrations averaged over ambient monitoring stations of each province (municipality) in the YRD region during January 2018. (For interpretation of the references to colour in this figure legend, the reader is referred to the web version of this article.)

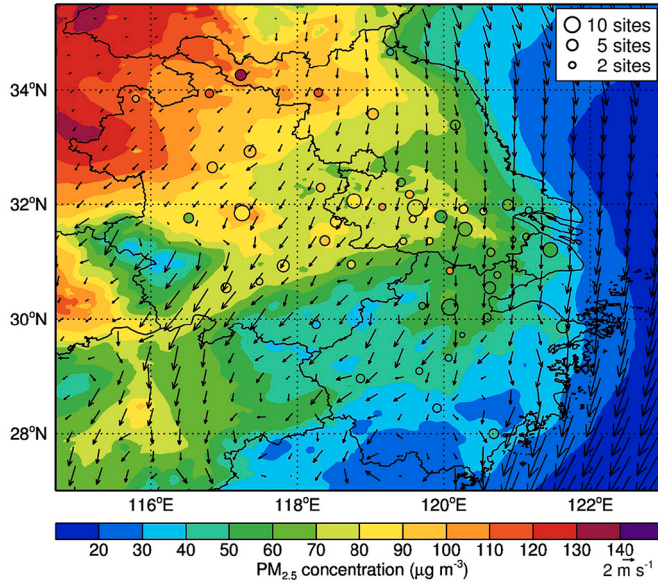


Fig. 3. Spatial distributions of simulated (colored shadings) and observed (colored dots) monthly mean $\text{PM}_{2.5}$ concentrations averaged over the study period in the simulation domain. Arrays show the simulated wind fields and the size of the circles indicates the number of observational stations in each city.

Lake station which represents the background air quality of the YRD region. During the study period, the measured $\text{PM}_{2.5}$ concentration at the Dianshan Lake station is about $69.75 \mu\text{g m}^{-3}$ on average. Fig. 4b and c show that the optical OC/EC concentrations are slightly higher than the thermal OC/EC concentrations, but the mass fractions of the main components in $\text{PM}_{2.5}$ incorporating these two methods highly agree with each other. The measurements clearly present that nitrate is the most important composition in ambient aerosols, followed by organics, sulfate, and ammonium, and EC accounts for about 4% of the total mass concentration. Likewise, the model simulation also shows that nitrate aerosol constitutes the largest contributor for the $\text{PM}_{2.5}$ concentration followed by organics (25%), sulfate (20%), and ammonium (18%), and the simulated EC fraction (3%) is moderately lower than the measurements.

In consideration of the complex processes in the atmosphere, the model simulation performs fairly well in reproducing the meteorological fields and haze pollution in the YRD region, which indicates that it can be used to further explore the influences of haze pollution on the regional thermal environment and the UHI.

3.2. Urban heat island effect

The spatial distributions of surface temperature and air temperature at 2 m averaged over the study period are shown in Fig. S9.

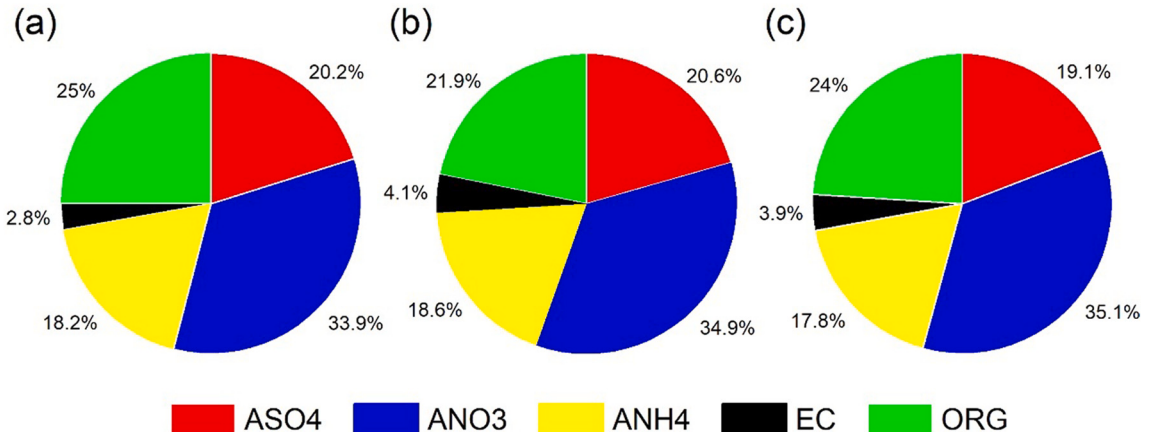


Fig. 4. A comparison between simulated (a) and measured (b, c) aerosol compositions of $\text{PM}_{2.5}$ at the Dianshan Lake station. The OC/EC concentrations in (b) and (c) are analyzed using the thermal and optical methods, respectively.

Both the surface temperature and air temperature exhibit an increasing trend from northwest to southeast across the YRD region. In comparison to the surface temperature, the air temperature is slightly lower, which should be attributed to the heating mechanism of the air by the underlying surface through longwave radiation. The various types of UHI effect over megacities of this region is calculated and summarized in Table 2. Using the urban buffer zone of a 6 km distance, the SUHII and CUHII averaged over the megacities are 0.99 °C and 0.50 °C, respectively, and higher UHII is found in Shanghai and Nanjing. In general, the CUHII is lower than the SUHII, which has been reported in previous studies (Hu et al., 2019; Du et al., 2021; Venter et al., 2021). Land surface directly receives short-wave radiation from the sun, and then heats the air above through emitting long-wave radiation. The air temperature is strongly modulated by the advection and vertical mixing processes of air mass in the boundary layer. These processes are more active during daytime than during nighttime, and consequently, the daytime UHI effect is usually slighter than the nighttime one, which is shown in our result and elsewhere (Yang et al., 2021). When adopting the administrative boundary as urban buffer zone, the derived UHII generally gets stronger (Table 2). This is because the buffer of administrative boundary is much larger than 6 km broadening from built-up areas, which includes more remote areas and hence the temperature is lower (Fig. 1).

The diurnal profiles of various UHII with $\pm 1\sigma$ are shown in Fig. 5. The SUHII is apparently higher than the CUHII throughout the day, and the difference between them varies with time. The most significant UHII appears in the evening (17:00–18:00 LT). In general, during the afternoon and the early night, the SUHII is much higher than the CUHII with fluctuant differences, linked to the active processes in the boundary layer. (Yang et al., 2022). During the late night, the differences remain large but almost consistent. Otherwise, much small differences occur at the morning hours, probably because both the surface and air cool down to the minimum temperature then. The selection of urban buffer areas can introduce minor differences in the assessment of the UHII, larger from the afternoon to the early night and smaller at the morning hours.

3.3. Effects of haze pollution on temperature and the UHI

Airborne particulate can exhibit radiative effects through absorbing and scattering incident solar radiation, which leads to changes in regional meteorological fields and hence in the UHI (Chen et al., 2018; Christoforou et al., 2000; Wang et al., 2021; Zhang et al., 2019). To probe into the influences of haze pollution on the UHII, we perform a sensitivity experiment in the model in terms of the aerosol-radiative forcing effect of PM_{2.5}.

The spatial distributions of changes in surface temperature and air temperature at 2 m resulted from the aerosol-radiative effects of PM_{2.5} are illustrated in Fig. 6. It should be noted that the temperature changes over water bodies are not presented here because of the higher specific heat capacity and hence the distinct feedbacks to ambient temperature changes compared to land surface. The presence of airborne aerosol leads to a ubiquitous decrease in both surface temperature and air temperature occur over the YRD region and the resulted decrease in surface temperature is generally more remarkable than air temperature. The most significant decrease in surface and air temperature reaches -1.55 °C and -0.99 °C. Because the direct source of surface warming is short-wave radiation, the radiative effect of aerosols generally reduces solar radiation reaching the surface, resulting in decrease in surface temperature (Suresh Babu et al., 2007; Huang et al., 2006; Córdoba-Jabonero et al., 2021). As a result, air temperature would also decrease due to surface cooling. Similar studies have been reported in existing studies (Sun et al., 2017; Wang et al., 2014; Zheng et al., 2018). For instance, Huang et al. (2006) pointed out that aerosols inhibit solar radiation, enhance downward long-wave radiation, and weaken surface warming during daytime and diurnal temperature variation. Zhang et al. (2009a) proposed that the local surface cooling effect of dust aerosols can be up to 1 °C in their study on the net radiative (both short- and long-wave) forcing of dust over East Asia.

The decrease in either surface temperature or air temperature shows an obvious spatial gradient from southeast to northwest across the YRD region. This spatial pattern is highly similar to the distribution of PM_{2.5} concentration in Fig. 3, highlighting the important perturbation of ambient PM_{2.5} in regional surface and air temperature. The relationships between temperature changes and ambient

Table 2

The average, daytime, and nighttime SUHII and CUHII over the YRD region and the main cities including Shanghai, Nanjing, Hangzhou, and Hefei. The UHI index is calculated as a difference in temperature (°C) between built-up areas and either a 6 km buffer zone or non-built-up areas within the administrative boundary.

Area	Average		Daytime		Nighttime	
	SUHII	CUHII	SUHII	CUHII	SUHII	CUHII
Urban buffer zone of a 6 km distance						
Shanghai	1.18	0.52	1.07	0.39	1.32	0.68
Nanjing	1.15	0.60	0.97	0.47	1.37	0.74
Hangzhou	0.88	0.49	0.85	0.45	0.91	0.54
Hefei	0.76	0.40	0.63	0.32	0.92	0.50
Mean	0.99	0.50	0.88	0.41	1.13	0.62
Urban buffer zone of the administrative boundary						
Shanghai	0.79	0.48	0.79	0.38	0.80	0.59
Nanjing	1.30	0.60	1.81	0.45	1.55	0.78
Hangzhou	1.69	0.88	1.42	0.74	2.03	1.05
Hefei	0.56	0.13	0.47	0.14	0.67	0.11
Mean	1.09	0.52	1.12	0.43	1.26	0.63

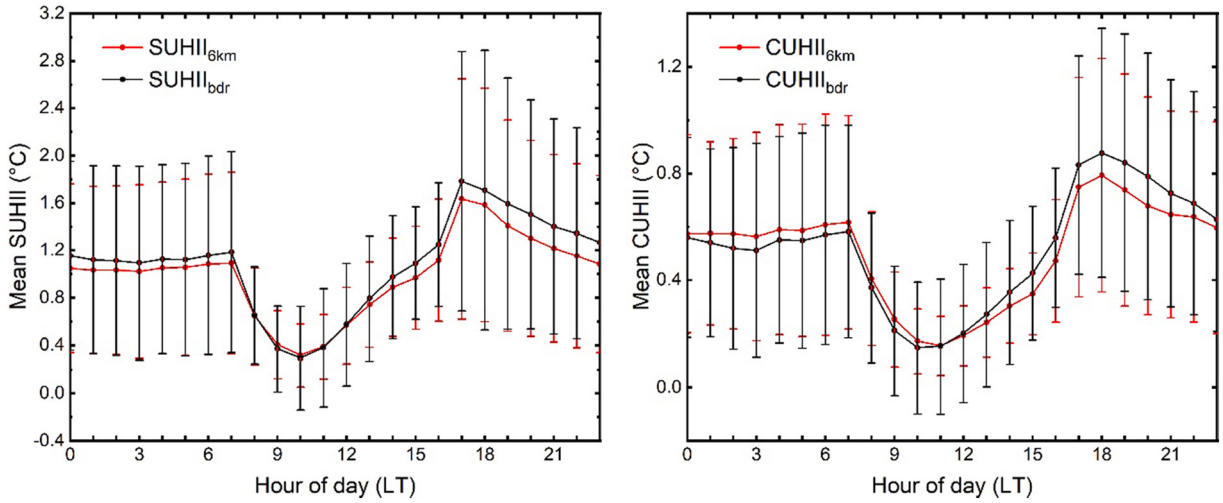


Fig. 5. Diurnal profiles of SUHII and CUHII with $\pm 1\sigma$ using the 6 km buffer zone and administrative boundary buffer zone in the YRD megacities during January 2018.

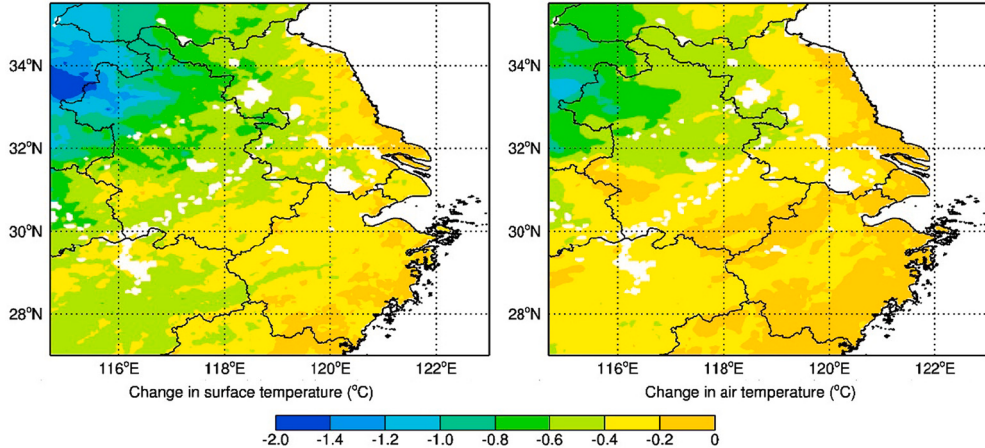


Fig. 6. Changes in monthly mean surface temperature and air temperature at 2 m over the YRD during the study period. Temperature changes over water bodies are excluded in the plots.

PM_{2.5} concentration over the grids of the study domain are presented in Fig. 7. Spatially, both the changes in surface temperature and the air temperature are negatively and nonlinearly correlated with PM_{2.5} concentration. Using nonlinear regressions, the correlation coefficient is -0.82 ($p < 0.01$) and -0.85 ($p < 0.01$), respectively. This result points to the fact that when PM_{2.5} concentration gets higher, the ambient temperature would decrease disproportionately over the YRD region.

The responses of SUHII/CUHII to the presence of airborne PM_{2.5} are presented in Fig. 8. The diurnal profiles of the changes in various types of the UHII show that ambient PM_{2.5} would lower the UHII throughout the day, but significant differences exist among different UHII indices. The changes in the SUHII are generally larger than those of the CUHII, particularly during the afternoon. The SUHII is directly associated with the incident solar radiation that heats the surface, while the CUHII is more closely linked to the emission of terrestrial longwave radiation from the heated underlying surface. In general, the resultant changes in the SUHII are two- or three-folds of the changes in the CUHII. Considering the measures of the urban buffer areas, the changes under the measure of the administrative boundary is greater than that of a 6 km distance. Using different urban buffers, the diurnal profiles show that the changes in the CUHII vary from almost zero to -0.06 °C and -0.11 °C, respectively. Slightly more changes occur during nighttime and the minimum changes appear at the morning hours (08:00–09:00 LT). As a comparison, the changes in the SUHII range from almost zero to -0.16 °C and -0.20 °C, respectively, with maximum changes in the afternoon.

3.4. Influences of various aerosol compositions

To further examine the aerosol-radiative effects of the main chemical compositions of PM_{2.5}, three more model sensitivity

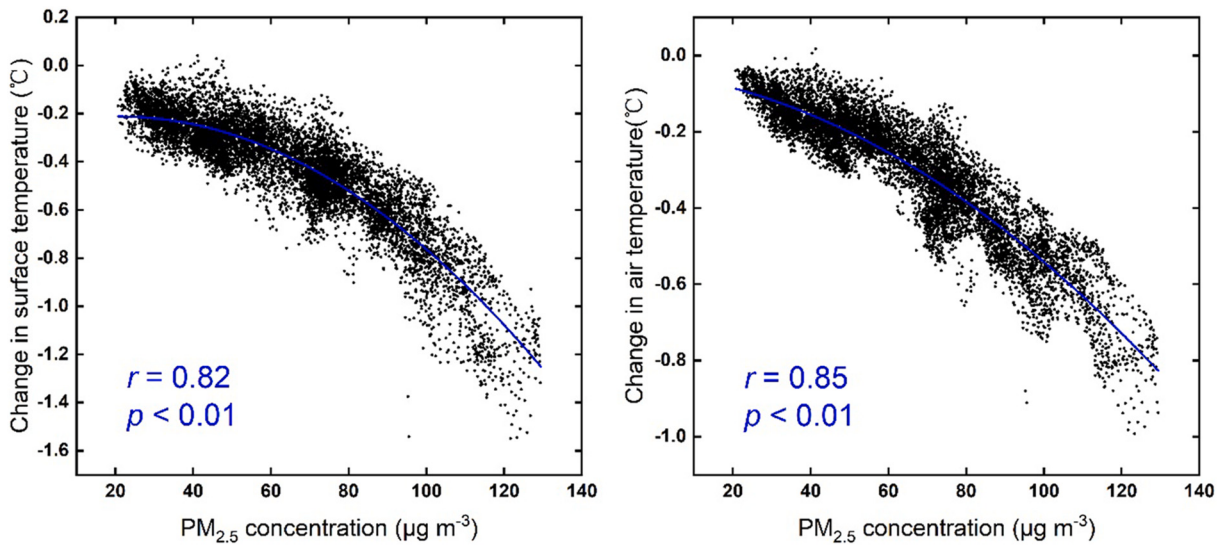


Fig. 7. Scatter plots showing the relationship between temperature change and $\text{PM}_{2.5}$ concentration in each grid cell over the study domain. The grid cells with a land cover type of water are not taken into account.

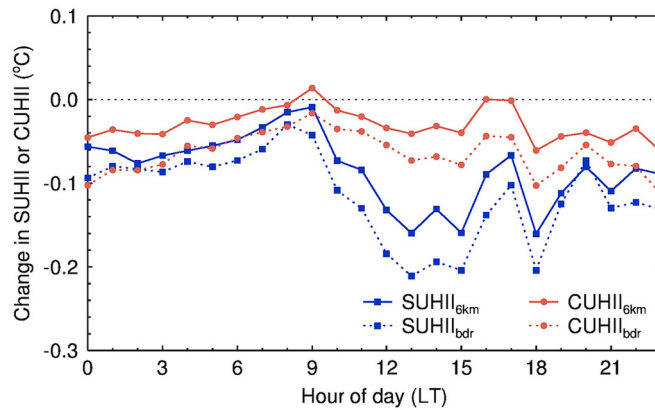


Fig. 8. Diurnal profiles of the changes in various types of the UHI over the YRD megacities.

experiments are conducted, which considers the effects of sulfate, nitrate, and ammonium aerosols (SNA), organic aerosols (ORG), and black carbon (BC). Detailed information about the model experiments is given in Table 3.

The spatial distributions of the influences of SNA, ORG, and BC on surface and air temperature at 2 m during daytime are demonstrated in Fig. 9, in which the radiative effect of various chemical compositions differs significantly from one another. SNA has a strong cooling effect on regional temperature, especially on surface temperature. The decrease in both surface and air temperature shows a southeast-northwest gradient across the study domain, and the most significant decreases of 1.57°C for surface temperature and 0.94°C for air temperature appear in the northwestern areas. In coastal areas, the surface and air temperature decreases only by less than 0.2°C and 0.4°C , respectively. A comparison with regional temperature changes resulted from $\text{PM}_{2.5}$ radiative effect in Fig. 6 suggests that SNA is the most important contributor to the total aerosol radiative effect in the YRD region. In contrast, the radiative

Table 3
Descriptions of model experiments.

Model simulation	Description
BASE	The aerosol-radiative effect of all aerosol species is on.
AREO	The aerosol-radiative effect of all aerosol species is off.
ARESNA0	The aerosol-radiative effect of sulfate, nitrate, and ammonium aerosols is off.
AREORG0	The aerosol-radiative effect of organic aerosols is off.
AREBC0	The aerosol-radiative effect of BC is off.

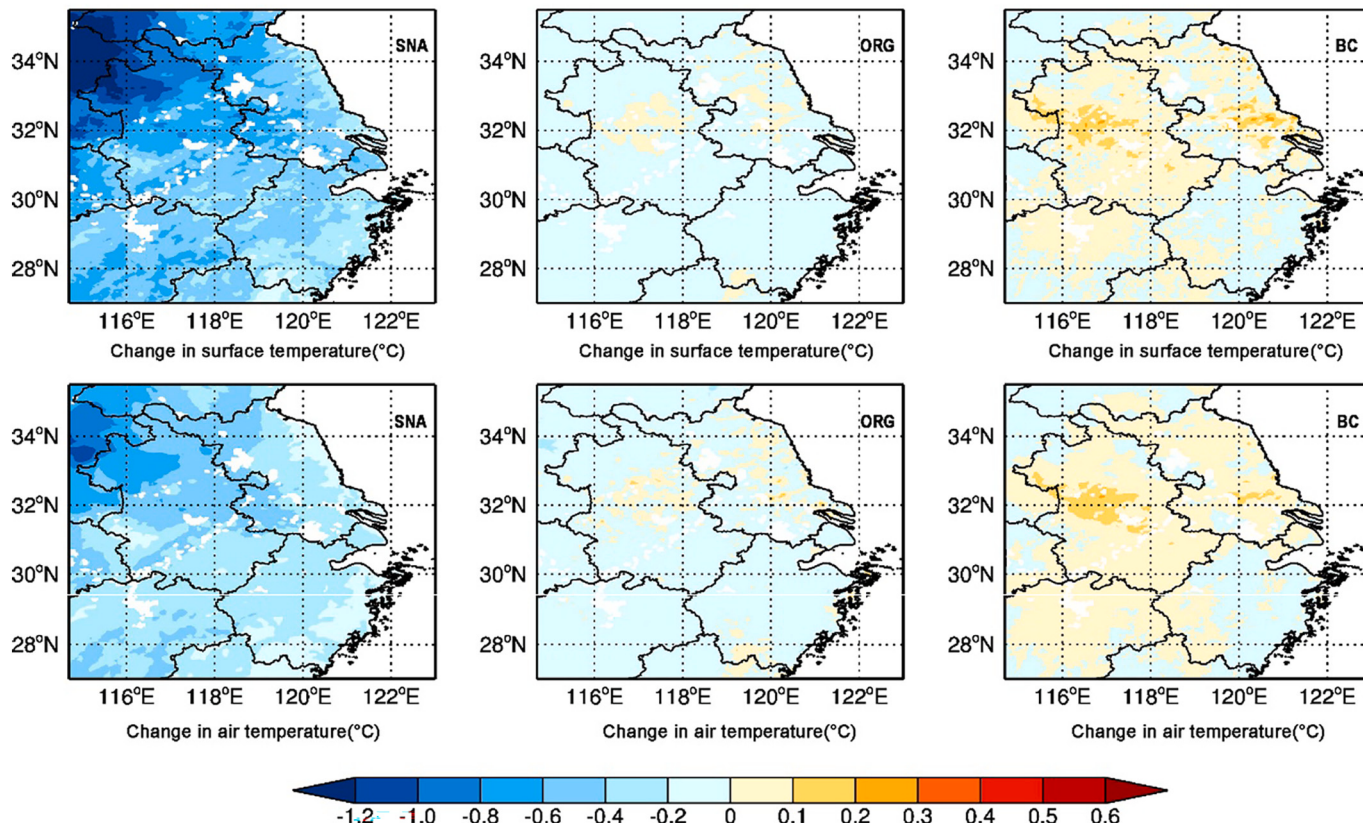


Fig. 9. The changes of daytime surface and air temperature caused by the radiative effect of SNA, ORG and BC in ambient PM_{2.5} over the YRD region in the study period.

effect of BC generally leads to an increase in surface and air temperature over the YRD region, particularly in Anhui and Jiangsu. The maximum surface and air temperature increase can reach around 0.2 °C. Considering the small mass fraction of BC in fine particulates, i.e., generally less than 5%, the resultant increase in ambient temperature is still considerable. The spatial distributions of temperature changes caused by the radiative effect of ORG are more complex. Over most areas of the YRD region, ORG presents a cooling effect, but exceptions (warming effect) also exist in some areas. In general, either the cooling effect or the warming effect of ORG is quite minor and even negligible, though ORG generally contributes largely to the total mass concentration.

Over the four megacities of the YRD, the radiative effects of various types of aerosols are similar. Fig. 10 illustrates the temperature changes averaged over different areas of the four megacities resulted from the radiative effect of PM_{2.5} and the main chemical compositions. T_u decreases by 0.63 °C and 0.34 °C for surface and the air, as a comparison, the decreases are 0.58 °C and 0.37 °C, respectively, for both $T_{6\text{km}}$ and T_{bdr} . This result shows an apparent difference in the radiative influence of aerosol on regional temperature between built-up and non-built-up areas. When analyzing the contributions from various types of aerosols over these megacities, we present that the aerosol radiative effect is predominantly caused by SNA and minorly attributed to ORG. BC, as the main absorbing aerosol in ambient particulates, exerts a weak warming effect over the megacities, which can only offset the cooling effect slightly.

The radiative effects of PM_{2.5} and the main chemical compositions on SUHII/CUHII are further assessed. Fig. 11 shows that the presence of airborne particulates, with scattering or absorbing radiative properties, would slightly suppress the UHII. Compared with the change in the CUHII, the suppression on the SUHII is generally stronger. Overall, the total PM_{2.5} mass loading reduces the SUHII by a range of 0.08 °C - 0.11 °C as indicated by using different urban buffers. As a comparison, the CUHII reduction resulted from the total PM_{2.5} is remarkably lower, ranging from 0.03 °C - 0.06 °C for different urban buffers. Among the various compositions of PM_{2.5}, SNA exhibits the dominant contributor in perturbing the UHI effect regardless of the selection of urban buffers. Although accounting for a large fraction of the total aerosol mass, ORG can only change the UHI effect minorly. In general, the change in the UHII owing to BC is negligible.

The radiative effects of ambient PM_{2.5} and the main compositions on vertical profiles of the CUHI are presented in Fig. S10. It is clear to see that the impact of PM_{2.5} is predominantly attributed to SNA, particularly at the heights of 100–200 m above the ground. If using the 6 km buffer, there is no significant difference among the baseline simulation and the various sensitivity experiments. While, if using the boundary buffer, we show remarkable differences in the radiative effects of ambient aerosols at different heights. Below the height of around 400 m, the presence of aerosols generally reduces the CUHI, and from 400 m to 800 m above the ground, it increases the CUHI. This result provides a novel perspective in understanding radiative effects of aerosols on the UHI.

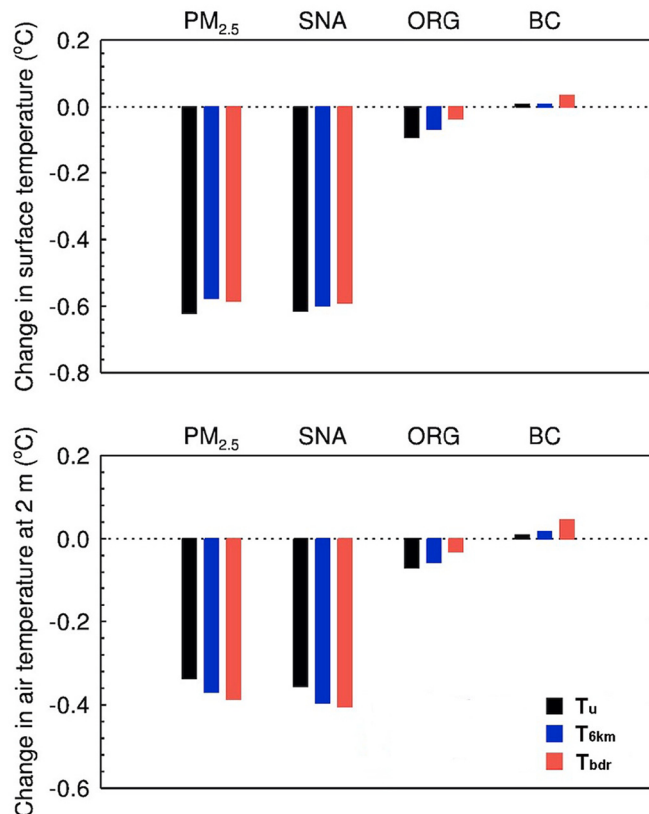


Fig. 10. Impacts of PM_{2.5} and the main compositions (SNA, ORG, and BC) on daytime surface and air temperature represented by T_u , $T_{6\text{km}}$ and T_{bdr} .

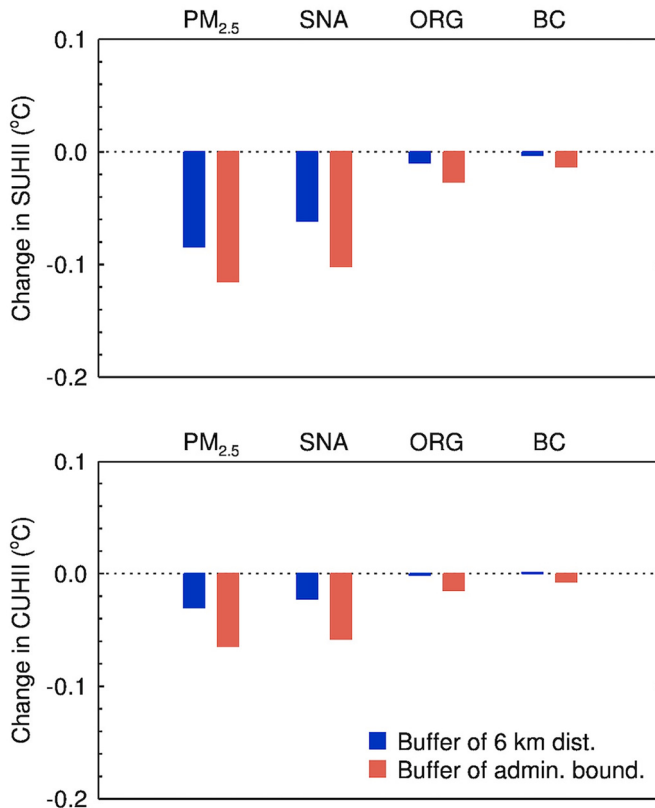


Fig. 11. Influences of PM_{2.5} and the main compositions (SNA, ORG, and BC) on daytime SUHII/CUHII using two types of urban buffers.

4. Conclusions

The YRD region is one of the most developed and urbanized regions in China with dense population. Haze pollution and the UHI phenomenon in this region have been reported in existing studies. However, the mechanisms underlying the evolution of the regional thermal environment and UHI are complex, which is still elusive. In the present study, we analyze the diurnal evolution of UHI in the YRD region during winter, and analyzes the influence of PM_{2.5} and the main components on regional thermal environment and UHI using the WRF-Chem model. The model performance in simulating meteorological fields, key gas-phase and aerosol pollutants is firstly validated against available measurements. Based on that, the aerosol-radiative effect on regional thermal environment and the UHI is discussed using model sensitivity experiments. The main conclusions are drawn as below.

- (1) A prevalent UHI effect exists in the study area, which is stronger during nighttime. The SUHII and CUHII exhibit similar diurnal profiles with maximum occurring around the evening (17:00–18:00 LT), and the SUHII is usually stronger than the CUHII. The selection of the urban buffer zone would influence the derived UHII remarkably, but can hardly change the diurnal profile of the UHII.
- (2) Aerosols have significant weakening effects on surface and air temperature, which fluctuates widely in the diurnal variation and gets stronger in the afternoon. The aerosol-radiative effect is more significant on the SUHII than on the CUHII.
- (3) The radiative effect of PM_{2.5} differs significantly among the components, but generally it suppresses the UHII. SNA is the most dominant contributor to the suppression. As a comparison, the cooling effect of ORG on the UHI is slight, and the effect of BC is negligible.

CRediT authorship contribution statement

Quan Zhang: Methodology, Formal analysis, Writing – original draft, Writing – review & editing. **Lang Liu:** Investigation, Writing – review & editing. **Gang Yang:** Writing – review & editing. **Weiwei Sun:** Investigation, Writing – review & editing. **Huimin Lu:** Writing – review & editing. **Tian Feng:** Conceptualization, Investigation, Methodology, Writing – review & editing.

Declaration of Competing Interest

The authors declare that they have no conflict of interest.

Data availability

Data will be made available on request.

Acknowledgments

This work was supported by the Natural Science Foundation of China (no. 42101339), the Natural Science Foundation of Zhejiang Province (no. LZ20D050001), the Public Projects of Ningbo City (no. 2021S089), the Natural Science Foundation of Ningbo (no. 2021J083), and the Science and Technology Innovation 2025 Major Project of Ningbo City (no. 2022Z032, 2021ZDZF020049), the Zhejiang Provincial Education Department Scientific Research Program Foundation (no. Y202043795).

Appendix A. Supplementary data

Supplementary data to this article can be found online at <https://doi.org/10.1016/j.uclim.2022.101354>.

References

- Athanasiopoulou, E., Vogel, H., Vogel, B., Tsimpidi, A.P., Pandis, S.N., Knote, C., Fountoukis, C., 2013. Modeling the meteorological and chemical effects of secondary organic aerosols during an Eucaari Campaign. *Atmos. Chem. Phys.* 13 (2), 625–645. <https://doi.org/10.5194/acp-13-625-2013>.
- Bhati, S., Mohan, M., 2015. WRF model evaluation for the urban heat Island assessment under varying land use/land cover and reference site conditions. *Theor. Appl. Clim.* 126 (1–2), 385–400. <https://doi.org/10.1007/s00704-015-1589-5>.
- Bi, J., Huang, J., Hu, Z., Holben, B.N., Guo, Z., 2014. Investigating the aerosol optical and radiative characteristics of heavy haze episodes in Beijing during January of 2013. *J. Geophys. Res. Atmos.* 119 (16), 9884–9900. <https://doi.org/10.1002/2014jd021757>.
- Binkowski, F.S., Roselle, S.J., 2003. Models-3 community multiscale air quality (CMAQ) model aerosol component 1. Model description. *J. Geophys. Res. Atmos.* 108 (D6) <https://doi.org/10.1029/2001jd001409>.
- Che, H.Z., 2005. Analysis of 40 years of solar radiation data from China, 1961–2000. *Geophys. Res. Lett.* 32 (6) <https://doi.org/10.1029/2004gl022322>.
- Chen, F., Dudhia, J., 2001. Coupling an advanced land surface-hydrology model with the penn state–NCAR mm5 modeling system. Part I: model implementation and sensitivity. *Mon. Weather Rev.* 129 (4), 569–585. [https://doi.org/10.1175/1520-0493\(2001\)129<0569:CAALSH>2.0.CO;2](https://doi.org/10.1175/1520-0493(2001)129<0569:CAALSH>2.0.CO;2).
- Chen, L., Zhang, M., Zhu, J., Wang, Y., Skorokhod, A., 2018. Modeling impacts of urbanization and urban heat Island mitigation on boundary layer meteorology and air quality in Beijing under different weather conditions. *J. Geophys. Res. Atmos.* 123 (8), 4323–4344. <https://doi.org/10.1002/2017jd027501>.
- Chen, S., Yang, Y., Deng, F., Zhang, Y., Liu, D., Liu, C., Gao, Z., 2022. A high-resolution monitoring approach of canopy urban heat Island using a random forest model and multi-platform observations. *Atmos. Meas. Tech.* 15 (3), 735–756. <https://doi.org/10.5194/amt-15-735-2022>.
- Cheng, L., Zhang, T., Chen, L., Li, L., Wang, S., Hu, S., Yuan, L., Wang, J., Wen, M., 2020. Investigating the impacts of urbanization on pm2.5 pollution in the Yangtze river delta of China: a spatial panel data approach. *Atmosphere-Basel* 11 (10). <https://doi.org/10.3390/atmos11101058>.
- Chew, L.W., Liu, X., Li, X.-X., Norford, L.K., 2021. Interaction between heat wave and urban heat Island: a case study in a Tropical Coastal city, Singapore. *Atmos. Res.* 247 <https://doi.org/10.1016/j.atmosres.2020.105134>.
- Chou, M.-D., Suarez, M.J., 1999. A Solar Radiation Parameterization for Atmospheric Studies (No. NASA/TM-1999-104606/VOL15).
- Chou, M.-D., Suarez, M.J., Liang, X.-Z., Yan, M.M.-H., Cote, C., 2001. A Thermal Infrared Radiation Parameterization for Atmospheric Studies (No. NASA/TM-2001-104606/VOL19).
- Christoforou, C.S., Salmon, L.G., Hannigan, M.P., Solomon, P.A., Cass, G.R., 2000. Trends in fine particle concentration and chemical composition in southern California. *J. Air Waste Manage. Assoc.* 50 (1), 43–53. <https://doi.org/10.1080/10473289.2000.10463985>.
- Clinton, N., Gong, P., 2013. Modis detected surface urban heat Islands and sinks: global locations and controls. *Remote Sens. Environ.* 134, 294–304. <https://doi.org/10.1016/j.rse.2013.03.008>.
- Córdoba-Jabonero, C., Sicard, M., López-Cayuela, M.-Á., Ansmann, A., Comerón, A., Zorzano, M.-P., Rodríguez-Gómez, A., Muñoz-Porcar, C., 2021. Aerosol radiative impact during the summer 2019 heatwave produced partly by an inter-continental saharan dust outbreak – Part 1: Short-wave dust direct radiative effect. *Atmos. Chem. Phys.* 21 (8), 6455–6479. <https://doi.org/10.5194/acp-21-6455-2021>.
- Cui, Y.Y., de Foy, B., 2012. Seasonal variations of the urban heat Island at the surface and the near-surface and reductions due to urban vegetation in Mexico City. *J. Appl. Meteorol. Climatol.* 51 (5), 855–868. <https://doi.org/10.1175/jamc-d-11-0104.1>.
- Deilami, K., Kamruzzaman, M., Liu, Y., 2018. Urban heat Island effect: a systematic review of spatio-temporal factors, data, methods, and mitigation measures. *Int. J. Appl. Earth Obs. Geoinf.* 67, 30–42. <https://doi.org/10.1016/j.jag.2017.12.009>.
- Diao, L., Zhang, H., Liu, B., Dai, C., Zhang, Y., Dai, Q., Bi, X., Zhang, L., Song, C., Feng, Y., 2021. Health risks of inhaled selected toxic elements during the haze episodes in Shijiazhuang, China: insight into critical risk sources. *Environ. Pollut.* 276, 116664 <https://doi.org/10.1016/j.envpol.2021.116664>.
- Donahue, N.M., Robinson, A.L., Stanier, C.O., Pandis, S.N., 2006. Coupled partitioning, dilution, and chemical aging of semivolatile organics. *Environ. Sci. Technol.* 40 (8), 2635–2643. <https://doi.org/10.1021/es052297c>.
- Du, Y., Xie, Z., Zeng, Y., Shi, Y., Wu, J., 2007. Impact of urban expansion on regional temperature change in the Yangtze River Delta. *J. Geogr. Sci.* 17 (4), 387–398. <https://doi.org/10.1007/s11442-007-0387-0>.
- Du, H., Zhan, W., Liu, Z., Li, J., Li, L., Lai, J., Miao, S., Huang, F., Wang, C., Wang, C., Fu, H., Jiang, L., Hong, F., Jiang, S., 2021. Simultaneous investigation of surface and canopy urban heat Islands over global cities. *ISPRS J. Photogramm. Remote Sens.* 181, 67–83. <https://doi.org/10.1016/j.isprsjprs.2021.09.003>.
- Estoque, R.C., Murayama, Y., Myint, S.W., 2017. Effects of landscape composition and pattern on land surface temperature: an urban heat Island study in the megacities of Southeast Asia. *Sci. Total Environ.* 577, 349–359. <https://doi.org/10.1016/j.scitotenv.2016.10.195>.
- Feng, T., Zhao, S., Zhang, X., Wang, Q., Liu, L., Li, G., Tie, X., 2020. Increasing wintertime ozone levels and secondary aerosol formation in the Guanzhong Basin, Central China. *Sci. Total Environ.* 745, 140961 <https://doi.org/10.1016/j.scitotenv.2020.140961>.
- Fenner, D., Meier, F., Scherer, D., Polze, A., 2014. Spatial and temporal air temperature variability in Berlin, Germany, during the years 2001–2010. *Urban Clim.* 10, 308–331. <https://doi.org/10.1016/j.uclim.2014.02.004>.

- Finessi, E., Decesari, S., Paglione, M., Giulianelli, L., Carbone, C., Gilardoni, S., Fuzzi, S., Saarikoski, S., Raatikainen, T., Hillamo, R., Allan, J., Mentel, T.F., Tiitta, P., Laaksonen, A., Petäjä, T., Kulmala, M., Worsnop, D.R., Facchini, M.C., 2012. Determination of the biogenic secondary organic aerosol fraction in the boreal forest by NMR spectroscopy. *Atmos. Chem. Phys.* 12 (2), 941–959. <https://doi.org/10.5194/acp-12-941-2012>.
- Gago, E.J., Roldan, J., Pacheco-Torres, R., Ordóñez, J., 2013. The city and urban heat Islands: a review of strategies to mitigate adverse effects. *Renew. Sust. Energ. Rev.* 25, 749–758. <https://doi.org/10.1016/j.rser.2013.05.057>.
- Grell, G.A., Peckham, S.E., Schmitz, R., McKeen, S.A., Frost, G., Skamarock, W.C., Eder, B., 2005. Fully coupled “online” chemistry within the WRF model. *Atmos. Environ.* 39 (37), 6957–6975. <https://doi.org/10.1016/j.atmosenv.2005.04.027>.
- Gu, Y., Wong, T.W., Law, C.K., Dong, G.H., Ho, K.F., Yang, Y., Yim, S.H.L., 2018. Impacts of sectoral emissions in China and the implications: air quality, public health, crop production, and economic costs. *Environ. Res. Lett.* 13 (8) <https://doi.org/10.1088/1748-9326/aad138>.
- Guenther, A., Karl, T., Harley, P., Wiedinmyer, C., Palmer, P.I., Geron, C., 2006. Estimates of global terrestrial isoprene emissions using Megan (model of emissions of gases and aerosols from nature). *Atmos. Chem. Phys.* 6 (11), 3181–3210. <https://doi.org/10.5194/acp-6-3181-2006>.
- Han, W., Li, Z., Wu, F., Zhang, Y., Guo, J., Su, T., Cribb, M., Fan, J., Chen, T., Wei, J., Lee, S.-S., 2020. The mechanisms and seasonal differences of the impact of aerosols on daytime surface urban heat Island effect. *Atmos. Chem. Phys.* 20 (11), 6479–6493. <https://doi.org/10.5194/acp-20-6479-2020>.
- He, J., Gong, S., Yu, Y., Yu, L., Wu, L., Mao, H., Song, C., Zhao, S., Liu, H., Li, X., Li, R., 2017. Air pollution characteristics and their relation to meteorological conditions during 2014–2015 in major Chinese cities. *Environ. Pollut.* 223, 484–496. <https://doi.org/10.1016/j.envpol.2017.01.050>.
- Hereher, M., Eissa, R., Alqasemi, A., El Kenawy, A.M., 2022. Assessment of air pollution at greater cairo in relation to the spatial variability of surface urban heat Island. *Environ. Sci. Pollut. Res. Int.* 29 (15), 21412–21425. <https://doi.org/10.1007/s11356-021-17383-9>.
- Horowitz, L.W., Walters, S., Mauzerall, D.L., Emmons, L.K., Rasch, P.J., Granier, C., Tie, X., Lamarque, J.-F., Schultz, M.G., Tyndall, G.S., Orlando, J.J., Brasseur, G.P., 2003. A global simulation of tropospheric ozone and related tracers: description and evaluation of Mozart, version 2. *J. Geophys. Res. Atmos.* 108 (D24), n/a-n/a. <https://doi.org/10.1029/2002jd002853>.
- Hu, L., Brunsell, N.A., 2015. A new perspective to assess the urban heat Island through remotely sensed atmospheric profiles. *Remote Sens. Environ.* 158, 393–406. <https://doi.org/10.1016/j.rse.2014.10.022>.
- Hu, Y., Hou, M., Jia, G., Zhao, C., Zhen, X., Xu, Y., 2019. Comparison of surface and canopy urban heat Islands within megacities of Eastern China. *ISPRS J. Photogramm. Remote Sens.* 156, 160–168. <https://doi.org/10.1016/j.isprsjprs.2019.08.012>.
- Huang, Y., Dickinson, R.E., Chameides, W.L., 2006. Impact of aerosol indirect effect on surface temperature over East Asia. *PNAS.* 103 (12), 4371–4376. <https://doi.org/10.1073/pnas.0504428103>.
- Janić, Z.I., 2002. Nonsingular implementation of the Mellor-Yamada level 2.5 scheme in the NCEP meso model (NCEP Office Note No. 437).
- Lai, J., Zhan, W., Huang, F., Voogt, J., Bechtel, B., Allen, M., Peng, S., Hong, F., Liu, Y., Du, P., 2018. Identification of typical diurnal patterns for clear-sky climatology of surface urban heat Islands. *Remote Sens. Environ.* 217, 203–220. <https://doi.org/10.1016/j.rse.2018.08.021>.
- Li, G., Zhang, R., Fan, J., Tie, X., 2005. Impacts of black carbon aerosol on photolysis and ozone. *J. Geophys. Res.* 110 (D23) <https://doi.org/10.1029/2005jd005898>.
- Li, G., Bei, N., Tie, X., Molina, L.T., 2011a. Aerosol effects on the photochemistry in Mexico City during mcma-2006/milagro campaign. *Atmos. Chem. Phys.* 11 (11), 5169–5182. <https://doi.org/10.5194/acp-11-5169-2011>.
- Li, G., Zavala, M., Lei, W., Tsimplidi, A.P., Karydis, V.A., Pandis, S.N., Canagaratna, M.R., Molina, L.T., 2011b. Simulations of organic aerosol concentrations in Mexico City using the WRF-chem model during the MCMA-2006/milagro campaign. *Atmos. Chem. Phys.* 11 (8), 3789–3809. <https://doi.org/10.5194/acp-11-3789-2011>.
- Li, G., Lei, W., Bei, N., Molina, L.T., 2012. Contribution of garbage burning to chloride and pm_{2.5} in Mexico City. *Atmos. Chem. Phys.* 12 (18), 8751–8761. <https://doi.org/10.5194/acp-12-8751-2012>.
- Li, X., Zhou, W., Ouyang, Z., 2013a. Relationship between land surface temperature and spatial pattern of greenspace: What are the effects of spatial resolution? *Landsc. Urban Plan.* 114, 1–8. <https://doi.org/10.1016/j.landurbplan.2013.02.005>.
- Li, Z.-L., Tang, B.-H., Wu, H., Ren, H., Yan, G., Wan, Z., Trigo, I.F., Sobrino, J.A., 2013b. Satellite-derived land surface temperature: current status and perspectives. *Remote Sens. Environ.* 131, 14–37. <https://doi.org/10.1016/j.rse.2012.12.008>.
- Li, M., Zhang, Q., Kurokawa, J.I., Woo, J.H., He, K., Lu, Z., Ohara, T., Song, Y., Streets, D.G., Carmichael, G.R., Cheng, Y., Hong, C., Huo, H., Jiang, X., Kang, S., Liu, F., Su, H., Zheng, B., 2017. Mix: a mosaic Asian anthropogenic emission inventory under the international collaboration framework of the Mics-Asia and HTAP. *Atmos. Chem. Phys.* 17 (2), 935–963. <https://doi.org/10.5194/acp-17-935-2017>.
- Li, H., Sodoudi, S., Liu, J., Tao, W., 2020. Temporal variation of urban aerosol pollution Island and its relationship with urban heat Island. *Atmos. Res.* 241 <https://doi.org/10.1016/j.atmosres.2020.104957>.
- Lin, Y.C., Hsu, S.C., Chou, C.C., Zhang, R., Wu, Y., Kao, S.J., Luo, L., Huang, C.H., Lin, S.H., Huang, Y.T., 2016. Wintertime haze deterioration in Beijing by industrial pollution deduced from trace metal fingerprints and enhanced health risk by heavy metals. *Environ. Pollut.* 208 (Pt A), 284–293. <https://doi.org/10.1016/j.jenvpol.2015.07.044>.
- Liousse, C., Penner, J.E., Chuang, C., Walton, J.J., Eddleman, H., Cachier, H., 1996. A global three-dimensional model study of carbonaceous aerosols. *J. Geophys. Res. Atmos.* 101 (D14), 19411–19432. <https://doi.org/10.1029/95jd03426>.
- McDonald, B.C., Goldstein, A.H., Harley, R.A., 2015. Long-term trends in California mobile source emissions and ambient concentrations of black carbon and organic aerosol. *Environ. Sci. Technol.* 49 (8), 5178–5188. <https://doi.org/10.1021/es505912b>.
- Miao, Y., Li, J., Miao, S., Che, H., Wang, Y., Zhang, X., Zhu, R., Liu, S., 2019. Interaction between planetary boundary layer and pm2.5 pollution in megacities in China: a review. *Curr. Pollut. Rep.* 5 (4), 261–271. <https://doi.org/10.1007/s40726-019-00124-5>.
- Ming, L., Jin, L., Li, J., Fu, P., Yang, W., Liu, D., Zhang, G., Wang, Z., Li, X., 2017. Pm2.5 in the Yangtze River Delta, China: chemical compositions, seasonal variations, and regional pollution events. *Environ. Pollut.* 223, 200–212. <https://doi.org/10.1016/j.envpol.2017.01.013>.
- Nenes, A., Pandis, S.N., Pilinis, C., 1998. Isorropia: a new thermodynamic equilibrium model for multiphase multicomponent inorganic aerosols. *Aquat. Geochem.* 4 (1), 123–152. <https://doi.org/10.1023/A:1009604003981>.
- Oke, T.R., 1982. The energetic basis of the urban heat Island. *Q. J. R. Meteorol. Soc.* 108 (455), 1–24.
- Peng, S., Piao, S., Ciais, P., Friedlingstein, P., Ottle, C., Breon, F.M., Nan, H., Zhou, L., Myneni, R.B., 2012. Surface urban heat Island across 419 global big cities. *Environ. Sci. Technol.* 46 (2), 696–703. <https://doi.org/10.1021/es2030438>.
- Peng, J., Xie, P., Liu, Y., Ma, J., 2016. Urban thermal environment dynamics and associated landscape pattern factors: a case study in the Beijing Metropolitan Region. *Remote Sens. Environ.* 173, 145–155. <https://doi.org/10.1016/j.rse.2015.11.027>.
- Pichieri, M., Bonafoni, S., Biondi, R., 2012. Satellite air temperature estimation for monitoring the canopy layer heat Island of Milan. *Remote Sens. Environ.* 127, 130–138. <https://doi.org/10.1016/j.rse.2012.08.025>.
- Poupkou, A., Nastos, P., Melas, D., Zerefos, C., 2011. Climatology of discomfort index and air quality index in a large urban mediterranean agglomeration. *Water Air Soil Pollut.* 222 (1–4), 163–183. <https://doi.org/10.1007/s11270-011-0814-9>.
- Qian, Y., Kaiser, D.P., Leung, L.R., Xu, M., 2006. More frequent cloud-free sky and less surface solar radiation in China from 1955 to 2000. *Geophys. Res. Lett.* 33 (1), n/a-n/a. <https://doi.org/10.1029/2005gl024586>.
- Qian, Y., Wang, W., Leung, L.R., Kaiser, D.P., 2007. Variability of solar radiation under cloud-free skies in China: the role of aerosols. *Geophys. Res. Lett.* 34 (12) <https://doi.org/10.1029/2006gl028800>.
- Robinson Allen, L., Donahue Neil, M., Shrivastava Manish, K., Weitkamp Emily, A., Sage Amy, M., Grieshop Andrew, P., Lane Timothy, E., Pierce Jeffrey, R., Pandis Spyros, N., 2007. Rethinking organic aerosols: semivolatile emissions and photochemical aging. *Science* 315 (5816), 1259–1262. <https://doi.org/10.1126/science.1133061>.
- Sang, J., Liu, H., Liu, H., Zhang, Z., 2000. Observational and numerical studies of wintertime urban boundary layer. *J. Wind Eng. Ind. Aerodyn.* 87 (2), 243–258. [https://doi.org/10.1016/S0167-6105\(00\)00040-4](https://doi.org/10.1016/S0167-6105(00)00040-4).
- Seinfeld, J.H., Pandis, S.N., 2006. *Atmospheric Chemistry and Physics - From Air Pollution to Climate Change*, 2nd ed. John Wiley & Sons, New Jersey.

- Shen, Z., Shi, J., Tan, J., Yang, H., 2020. The migration of the warming center and urban heat Island effect in Shanghai during urbanization. *Front. Earth. Sc.-Switz.* 8 <https://doi.org/10.3389/feart.2020.00340>.
- Sheng, L., Tang, X., You, H., Gu, Q., Hu, H., 2017. Comparison of the urban heat Island intensity quantified by using air temperature and landsat land surface temperature in Hangzhou, China. *Ecol. Indic.* 72, 738–746. <https://doi.org/10.1016/j.ecolind.2016.09.009>.
- Singh, V.K., Mughal, M.O., Martilli, A., Acerro, J.A., Ivanchev, J., Norford, L.K., 2022. Numerical analysis of the impact of anthropogenic emissions on the urban environment of Singapore. *Sci. Total Environ.* 806 (Pt 2), 150534 <https://doi.org/10.1016/j.scitotenv.2021.150534>.
- Slater, J., Coe, H., McFiggans, G., Tonttila, J., Romakkaniemi, S., 2022. The effect of BC on aerosol-boundary layer feedback: potential implications for urban pollution episodes. *Atmos. Chem. Phys.* 22 (4), 2937–2953. <https://doi.org/10.5194/acp-22-2937-2022>.
- Song, Z., Li, R., Qiu, R., Liu, S., Tan, C., Li, Q., Ge, W., Han, X., Tang, X., Shi, W., Song, L., Yu, W., Yang, H., Ma, M., 2018. Global land surface temperature influenced by vegetation cover and pm2.5 from 2001 to 2016. *Remote Sens.* 10 (12) <https://doi.org/10.3390/rs10122034>.
- Song-You, H., Jeong-Ock Jade, L., 2006. The WRF single-moment 6-class microphysics scheme (wsm6). *Asia-Pac. J. Atmos. Sci.* 42, 129–151.
- Sulong, N.A., Latif, M.T., Khan, M.F., Amil, N., Ashfold, M.J., Wahab, M.I.A., Chan, K.M., Sahani, M., 2017. Source apportionment and health risk assessment among specific age groups during haze and non-haze episodes in Kuala Lumpur, Malaysia. *Sci. Total Environ.* 601–602, 556–570. <https://doi.org/10.1016/j.scitotenv.2017.05.153>.
- Sun, Y., Song, T., Tang, G., Wang, Y., 2013. The vertical distribution of pm2.5 and boundary-layer structure during summer haze in Beijing. *Atmos. Environ.* 74, 413–421. <https://doi.org/10.1016/j.atmosenv.2013.03.011>.
- Sun, K., Liu, H., Wang, X., Peng, Z., Xiong, Z., 2017. The aerosol radiative effect on a severe haze episode in the Yangtze River Delta. *J. Meteorol. Res.-Prc.* 31 (5), 865–873. <https://doi.org/10.1007/s13351-017-7007-4>.
- Sun, W., Wang, D., Yao, L., Fu, H., Fu, Q., Wang, H., Li, Q., Wang, L., Yang, X., Xian, A., Wang, G., Xiao, H., Chen, J., 2019. Chemistry-triggered events of pm2.5 explosive growth during late autumn and winter in Shanghai, China. *Environ. Pollut.* 254 (Pt A), 112864 <https://doi.org/10.1016/j.envpol.2019.07.032>.
- Suresh Babu, S., Krishna Moorthy, K., Sathesh, S.K., 2007. Temporal heterogeneity in aerosol characteristics and the resulting radiative impacts at a tropical coastal station – Part 2: direct short wave radiative forcing. *Ann. Geophys.* 25, 2309–2320. <https://doi.org/10.5194/angeo-25-2309-2007>.
- Tie, X., Madronich, S., Walters, S., Zhang, R., Rasch, P., Collins, W., 2003. Effect of clouds on photolysis and oxidants in the troposphere. *J. Geophys. Res.* 108 (D20) <https://doi.org/10.1029/2003jd003659>.
- Tiwari, S., Bisht, D.S., Srivastava, A.K., Pipal, A.S., Taneja, A., Srivastava, M.K., Attri, S.D., 2014. Variability in atmospheric particulates and meteorological effects on their mass concentrations over Delhi, India. *Atmos. Res.* 145–146, 45–56. <https://doi.org/10.1016/j.atmosres.2014.03.027>.
- Venter, Z.S., Chakraborty, T., Lee, X., 2021. Crowdsourced air temperatures contrast satellite measures of the urban heat Island and its mechanisms. *Sci. Adv.* 7 (22), eabb9569. <https://doi.org/10.1126/sciadv.eabb9569>.
- Volkamer, R., San Martini, F., Molina, L.T., Salcedo, D., Jimenez, J.L., Molina, M.J., 2007. A missing sink for gas-phase glyoxal in Mexico City: formation of secondary organic aerosol. *Geophys. Res. Lett.* 34 (19) <https://doi.org/10.1029/2007GL030752>.
- Wang, J., Wang, S., Jiang, J., Ding, A., Zheng, M., Zhao, B., Wong, D.C., Zhou, W., Zheng, G., Wang, L., Pleim, J.E., Hao, J., 2014. Impact of aerosol-meteorology interactions on fine particle pollution during China's severe haze episode in January 2013. *Environ. Res. Lett.* 9 (9) <https://doi.org/10.1088/1748-9326/9/9/094002>.
- Wang, K., Jiang, S., Wang, J., Zhou, C., Wang, X., Lee, X., 2017. Comparing the diurnal and seasonal variabilities of atmospheric and surface urban heat Islands based on the Beijing Urban meteorological network. *J. Geophys. Res. Atmos.* 122 (4), 2131–2154. <https://doi.org/10.1002/2016jd025304>.
- Wang, L., Li, D., Zhang, N., Sun, J., Guo, W., 2020. Surface urban heat and cool Islands and their drivers: an observational study in Nanjing, China. *J. Appl. Meteorol. Climatol.* 59 (12), 1987–2000. <https://doi.org/10.1175/jamc-d-20-0089.1>.
- Wang, Y., Guo, Z., Han, J., 2021. The relationship between urban heat Island and air pollutants and them with influencing factors in the Yangtze River Delta, China. *Ecol. Indic.* 129 <https://doi.org/10.1016/j.ecolind.2021.107976>.
- Wang, J., Ge, X., Sonya, C., Ye, J., Lei, Y., Chen, M., Zhang, Q., 2022. Influence of regional emission controls on the chemical composition, sources, and size distributions of submicron aerosols: insights from the 2014 Nanjing Youth Olympic Games. *Sci. Total Environ.* 807 (Pt 2), 150869 <https://doi.org/10.1016/j.scitotenv.2021.150869>.
- Wesely, M., 2007. Parameterization of surface resistances to gaseous dry deposition in regional-scale numerical models. *Atmos. Environ.* 41, 52–63. <https://doi.org/10.1016/j.atmosenv.2007.10.058>.
- Xing, C., Liu, C., Wang, S., Chan, K.L., Gao, Y., Huang, X., Su, W., Zhang, C., Dong, Y., Fan, G., Zhang, T., Chen, Z., Hu, Q., Su, H., Xie, Z., Liu, J., 2017. Observations of the vertical distributions of summertime atmospheric pollutants and the corresponding ozone production in Shanghai, China. *Atmos. Chem. Phys.* 17 (23), 14275–14289. <https://doi.org/10.5194/acp-17-14275-2017>.
- Xu, L., Penner, J.E., 2012. Global simulations of nitrate and ammonium aerosols and their radiative effects. *Atmos. Chem. Phys.* 12 (20), 9479–9504. <https://doi.org/10.5194/acp-12-9479-2012>.
- Yang, Y., Zheng, Z., Yim, S.Y.L., Roth, M., Ren, G., Gao, Z., Wang, T., Li, Q., Shi, C., Ning, G., Li, Y., 2020a. pm2.5 pollution modulates wintertime urban heat Island intensity in the Beijing-Tianjin-Hebei Megalopolis, China. *Geophys. Res. Lett.* 47 (1) <https://doi.org/10.1029/2019gl084288>.
- Yang, Y., Zhang, M., Li, Q., Chen, B., Gao, Z., Ning, G., Liu, C., Li, Y., Luo, M., 2020b. Modulations of surface thermal environment and agricultural activity on intraseasonal variations of summer diurnal temperature range in the Yangtze River Delta of China. *Sci. Total Environ.* 736, 139445 <https://doi.org/10.1016/j.scitotenv.2020.139445>.
- Yang, G., Ren, G., Zhang, P., Xue, X., Tysa, S.K., Jia, W., Qin, Y., Zheng, X., Zhang, S., 2021. Pm 2.5 influence on Urban Heat Island (UHI) effect in Beijing and the possible mechanisms. *J. Geophys. Res. Atmos.* 126, 17. <https://doi.org/10.1029/2021jd035227>.
- Yang, Y., Guo, M., Ren, G., Liu, S., Zong, L., Zhang, Y., Zheng, Z., Miao, Y., Zhang, Y., 2022. Modulation of wintertime Canopy Urban Heat Island (CUHI) intensity in Beijing by synoptic weather pattern in planetary boundary layer. *J. Geophys. Res. Atmos.* 127, 8. <https://doi.org/10.1029/2021jd035988>.
- Yao, R., Wang, L., Huang, X., Niu, Y., Chen, Y., Niu, Z., 2018. The influence of different data and method on estimating the surface urban heat Island intensity. *Ecol. Indic.* 89, 45–55. <https://doi.org/10.1016/j.ecolind.2018.01.044>.
- Zhan, C., Xie, M., 2022. Land use and anthropogenic heat modulate ozone by meteorology: a perspective from the Yangtze River Delta Region. *Atmos. Chem. Phys.* 22 (2), 1351–1371. <https://doi.org/10.5194/acp-22-1351-2022>.
- Zhang, D.F., Zakey, A.S., Gao, X.J., Giorgi, F., Solmon, F., 2009a. Simulation of dust aerosol and its regional feedbacks over East Asia using a regional climate model. *Atmos. Chem. Phys.* 9, 1095–1110. <https://doi.org/10.5194/acp-9-1095-2009>.
- Zhang, Q., Streets, D.G., Carmichael, G.R., He, K.B., Huo, H., Kannari, A., Klimont, Z., Park, I.S., Reddy, S., Fu, J.S., Chen, D., Duan, L., Lei, Y., Wang, L.T., Yao, Z.L., 2009b. Asian emissions in 2006 for the NASA intex-b mission. *Atmos. Chem. Phys.* 9 (14), 5131–5153. <https://doi.org/10.5194/acp-9-5131-2009>.
- Zhang, X., Xu, X., Ding, Y., Liu, Y., Zhang, H., Wang, Y., Zhong, J., 2019. The impact of meteorological changes from 2013 to 2017 on pm2.5 mass reduction in key regions in China. *Sci. China Earth Sci.* 62 (12), 1885–1902. <https://doi.org/10.1007/s11430-019-9343-3>.
- Zhang, F., Wang, Y., Peng, J., Chen, L., Sun, Y., Duan, L., Ge, X., Li, Y., Zhao, J., Liu, C., Zhang, X., Zhang, G., Pan, Y., Wang, Y., Zhang, A.L., Ji, Y., Wang, G., Hu, M., Molina, M.J., Zhang, R., 2020. An unexpected catalyst dominates formation and radiative forcing of regional haze. *Proc. Natl. Acad. Sci. U. S. A.* 117 (8), 3960–3966. <https://doi.org/10.1073/pnas.1919343117>.
- Zhang, Q., Wu, Z., Singh, V.P., Liu, C., 2021a. Impacts of spatial configuration of land surface features on land surface temperature across urban agglomerations, China. *Remote Sens.* 13 (19) <https://doi.org/10.3390/rs13194008>.
- Zhang, X., Feng, T., Zhao, S., Yang, G., Zhang, Q., Qin, G., Liu, L., Long, X., Sun, W., Gao, C., Li, G., 2021b. Elucidating the impacts of rapid urban expansion on air quality in the Yangtze River Delta, China. *Sci. Total Environ.* 799, 149426 <https://doi.org/10.1016/j.scitotenv.2021.149426>.
- Zhang, R., Chen, Q., Li, G., Guo, W., Liu, X., Zhu, Y., Xia, J., 2022. Synergistic effects of air pollutants on meteorological fields at the junction of the Loess Plateau, Mongolian Plateau and Tibetan Plateau over Northwest China during summer. *Atmos. Res.* 267 <https://doi.org/10.1016/j.atmosres.2021.105921>.
- Zhao, J., Levitt, N.P., Zhang, R., Chen, J., 2006. Heterogeneous reactions of methylglyoxal in acidic media: implications for secondary organic aerosol formation. *Environ. Sci. Technol.* 40 (24), 7682–7687. <https://doi.org/10.1021/es060610k>.

- Zheng, Z., Ren, G., Wang, H., Dou, J., Gao, Z., Duan, C., Li, Y., Ngarukiyimana, J.P., Zhao, C., Cao, C., Jiang, M., Yang, Y., 2018. Relationship between fine-particle pollution and the urban heat Island in Beijing, China: observational evidence. *Bound.-Layer Meteorol.* 169 (1), 93–113. <https://doi.org/10.1007/s10546-018-0362-6>.
- Zhong, S., Qian, Y., Zhao, C., Leung, R., Wang, H., Yang, B., Fan, J., Yan, H., Yang, X.-Q., Liu, D., 2017a. Urbanization-induced urban heat Island and aerosol effects on climate extremes in the Yangtze River Delta Region of China. *Atmos. Chem. Phys.* 17 (8), 5439–5457. <https://doi.org/10.5194/acp-17-5439-2017>.
- Zhou, J., Chen, Y., Zhang, X., Zhan, W., 2013. Modelling the diurnal variations of urban heat Islands with multi-source satellite data. *Int. J. Remote Sens.* 34 (21), 7568–7588. <https://doi.org/10.1080/01431161.2013.821576>.
- Zhou, D., Zhao, S., Liu, S., Zhang, L., Zhu, C., 2014. Surface urban heat Island in China's 32 major cities: spatial patterns and drivers. *Remote Sens. Environ.* 152, 51–61. <https://doi.org/10.1016/j.rse.2014.05.017>.
- Zhou, D., Xiao, J., Bonafoni, S., Berger, C., Deilami, K., Zhou, Y., Frolking, S., Yao, R., Qiao, Z., Sobrino, J., 2018. Satellite remote sensing of surface urban heat Islands: progress, challenges, and perspectives. *Remote Sens.* 11 (1) <https://doi.org/10.3390/rs11010048>.